Design and synthesis of optimized SOFC structures

Jingyu Shi, Frank M. Zalar, and Henk Verweij

Department of Materials Science & Engineering, Ohio State University, 2041 College Road, Columbus OH 43210-1178, USA
Internet: www.mse.eng.ohio-state.edu/fac_staff/faculty/verweij/

Abstract

State-of-the-art Solid Oxide Fuel Cell (SOFC) designs have an Yttria-stabilized Zirconia (YSZ) electrolyte, a Lanthanum-Strontium Manganate cathode and a Ni-YSZ composite anode. SOFC charge transfer reactions are generally assumed to occur at triple-phase-boundaries (TPB's) between electrode, electrolyte and gas phase. Equilibrium space-charge-accumulation lengths suggest the width of the TPB to be in the order of 10 nm. The efficiency of SOFC conversion is most likely affected by:

- Resistive losses in the bulk electrolyte, including constriction effects due to the fact that charge transfer occurs at narrow TPB's only.
- Surface charge transfer at the TPB.

A TPB of only 10 nm thick naturally leads to the suggestion that typical dimensions of cathode and anode material and porosity should also be of the order of 10 nm to obtain the best possible electrode efficiency. In the ideal electrode/electrolyte interface there are many active triple phase boundary contacts, possibly percolating into the porous electrode structure. Further away from the electrolyte interface, both cathode and anode may coarsen to allow for an optimum strength, gas transport and electron conductivity. An electrolyte thickness also in the order of 10 nm is achievable by stretching the limits of what is possible with high definition colloidal processing. Optimized structures as described will result in much better performance at lower temperatures but also require much better control of particle morphology. A graded interface between the porous electrode structure and the dense electrolyte structure is likely to result in better adhesion and thermo-chemical stability during lifetime.

Design and realization of optimized SOFC structures is a major enterprise that requires a concerted effort of several research groups with special attention for the relation morphology-properties-synthesis. This paper discusses quantitative descriptions of SOFC transport phenomena that can be used as a starting point to develop optimized cell designs. A finite element description is presented of solid state transport of charge carriers, based on Langmuir lattice statistics, Onsager linear irreversible thermodynamics and the Poisson equation. In addition, unconventional strategies will be presented for realizing the foreseen, ideal graded structures with thin electrolytes. The example is presented of synthesis and consolidation of <10 nm spherical zirconia particles by modified emulsion precipitation. The particles are formed in the confinement of aqueous solution droplets in a normal emulsion, followed by removal of water and subsequent steric stabilization of the particles in the remaining oil medium. The particles, surrounded by their organic polymer stabilizer, are deposited as a thin filtration layer on a meso-porous substrate, followed by removal of the polymer by O_2 plasma oxidation. This treatment results in complete densification of the particle layer at, apparently, near room temperature conditions. The final crystal structure is

then formed by crystallization around 600ºC. This temperature is sufficiently low to preserve originally designed 10 nm details.

Modeling

In general, the mass flux of a species is proportional its concentration and velocity as

$$J_I = C_I v_I \tag{1}$$

The velocity of a species is proportional to its mobility and the average force acting upon it as

$$v_I = B_I \bar{F} \tag{2}$$

From Onsager linear irreversible thermodynamics, the flux of a species with no other mobile species present is proportional to the gradient in its chemical potential, $\tilde{\mu}_I$, as

$$J_I = -L_I \nabla \tilde{\mu}_I \tag{3}$$

By comparison of (3) with (1) and (2), it is observed that $\bar{F} = -\nabla \tilde{\mu}_I$ and $L_I = B_I C_I$ resulting in

$$J_I = -B_I C_I \nabla \tilde{\mu}_I \tag{4}$$

For charged species, the chemical potential is often described as the electrochemical potential and written as the sum of a chemical term and a field term:

$$\tilde{\mu}_I = \mu_I + z_I q_{el} \Phi \tag{5}$$

μ_I, is comprised of non-configurational and configurational contributions. The non-configurational part of the chemical potential includes the species' enthalpy and non-configurational entropy contributions. The configuration dependent part of the chemical potential is desribed in the simplest approach by Langmuir lattice statistics. The total electrochemical potential is then expressed as

$$\tilde{\mu}_I = \mu_I^0 + k_B T \ln\left(\frac{\theta_I}{1-\theta_I}\right) + z_I q_{el} \Phi \tag{6}$$

All non-configurational contributions are included in μ_I^0, and θ_I is the average lattice site occupation fraction. The denominator in the logarithm modifies the configurational entropy by accounting explicitly for the unoccupied lattice sites.

The species' concentration is given in terms of θ_I as $C_I = C_L \theta_I$, where C_L is the concentration of lattice sites. The species' mobility is also given in terms of θ_I as $B_I = \tilde{f}_L B_I^0 (1-\theta_I)$, where $\tilde{f}_L$ is a correlation factor for the lattice, L, and B_I^0 is the species' unconditional mobility. Unconditional mobility is defined as the mobility when all possible transport paths are available.

With the formulation and definitions above, the diffusion equation has the form

$$\frac{\partial C_I}{\partial t} + \nabla \cdot \left(-B_I C_I \nabla \tilde{\mu}_I \right) = 0 \tag{7}$$

which upon substitution reduces to

$$C_L \frac{\partial \theta_I}{\partial t} + \nabla \cdot \left(-\tilde{f}_L B_I^0 C_L \mathrm{k_B} T \nabla \theta_I - \tilde{f}_L B_I^0 \left(1-\theta_I\right) C_L \theta_I z_I \mathrm{q_{el}} \nabla \Phi \right) = 0 \tag{8}$$

From inspection of (8), it is easily observed that the flux is a combination of diffusion with $D_I = \tilde{f}_L B_I^0 \mathrm{k_B} T$ and electric migration with $\sigma_I = \tilde{f}_L B_I^0 \left(1-\theta_I\right) C_L \theta_I z_I \mathrm{q_{el}}$.

The electrostatic potential is coupled to the local concentration of charged particles through the Poisson equation

$$\nabla \cdot \left(-\varepsilon \nabla \Phi \right) = \rho_\mathrm{q} \tag{9}$$

The charge density, ρ_q, is the sum $\sum z_I \mathrm{q_{el}} C_I$ over all charged species.

The basic design of a SOFC is an electrolyte membrane sandwiched between two electrodes. The electrolyte and electrodes may be made of many different materials, and the electrodes can be fabricated with several different morphologies. Here a simple one-dimensional SOFC acting as an oxygen cell is explored. The electrolyte is considered to be 8 mol% yttria stabilized zirconia (YSZ) with composition $(Zr_{0.851852},Y_{0.148148})O_{1.925926}$. The cathode and anode are considered to be dense lanthanum strontium cobalt ferrites with compositions $(La_{0.7},Sr_{0.3})(Co^{3+}{}_{0.8},Fe^{2+}{}_{0.2})O_{2.75}$ and $(La_{0.7},Sr_{0.3})(Co^{3+}{}_{0.9},Fe^{2+}{}_{0.1})O_{2.71355}$, respectively.

The modeled domain is composed of 3 sub-domains: an electrolyte sub-domain and 2 electrode sub-domains. A diffusion equation for the transport of oxide ions and a Poisson equation coupling the electrostatic potential and local charge density are defined on the electrolyte sub-domain. A diffusion equation for the transport of oxide ions, a diffusion equation for the transport of localized electrons, and a Poisson equation coupling the electrostatic potential and local charge density are defined on the electrode subdomains.

The modeled domain has 4 boundaries – 2 internal boundaries between the electrodes and electrolyte subdomains and 2 external boundaries. At the internal boundaries, oxide ions may transfer from electrode to electrolyte or from electrolyte to electrode. This transfer is governed by a Butler-Volmer type flux from electrode to electrolyte given as

$$J_{\mathrm{O}^{2-},Ode \rightarrow Yte} = \bar{C}_{Ode/Yte} \left\{ \vec{k} \theta_{\mathrm{O}^{2-},Ode} \left(1-\theta_{\mathrm{O}^{2-},Yte}\right) - \overleftarrow{k} \theta_{\mathrm{O}^{2-},Yte} \left(1-\theta_{\mathrm{O}^{2-},Ode}\right) \right\} \tag{10}$$

where the rates are given as

$$k^0 = \frac{\mathrm{k_B}T}{\mathrm{h}} \tag{11}$$

$$\vec{k} = k^0 \exp\left\{-\frac{U^{\mathrm{act}} + \beta z_{\mathrm{O}^{2-}} \mathrm{q_{el}}\left(\Phi_{Yte} - \Phi_{Ode}\right)}{\mathrm{k_B}T}\right\} \tag{12}$$

$$\overleftarrow{k} = k^0 \exp\left\{-\frac{U^{\mathrm{act}} - (1-\beta) z_{\mathrm{O}^{2-}} \mathrm{q_{el}}\left(\Phi_{Yte} - \Phi_{Ode}\right)}{\mathrm{k_B}T}\right\} \tag{13}$$

At the external boundaries, oxide ions may be incorporated from or released into the ambient gas atmosphere. It is assumed that the atmosphere instantaneously establishes and maintains an equilibrium adsorbed surface layer of monatomic oxygen according to the reaction

$$\frac{1}{2}\mathrm{O_2} + \mathrm{V_O} \rightleftarrows \mathrm{O_O} \tag{14}$$

The concentration of this layer is determined from the above reaction's equilibrium reaction quotient

$$K_{\mathrm{ads}} = \frac{\theta_{\mathrm{O},Ode/g}}{\sqrt{p_{\mathrm{O_2}}}\left(1-\theta_{\mathrm{O},Ode/g}\right)} \tag{15}$$

yielding

$$\theta_{\mathrm{O},Ode/g} = \frac{K_{\mathrm{ads}}\sqrt{p_{\mathrm{O_2}}}}{1+K_{\mathrm{ads}}\sqrt{p_{\mathrm{O_2}}}} \tag{16}$$

The monatomic oxygen from the surface layer is incorporated into the electrodes or oxide ions from the electrodes are released into the adsorbed surface layer similarly to (10) as

$$J_{\mathrm{O}^{2-},Ode\rightarrow Ode/g} = \bar{C}_{Ode/g}\left\{\vec{k}\theta_{\mathrm{O}^{2-},Ode}\left(1-\theta_{\mathrm{O}^{2-},Ode/g}\right)\left(1-\theta_{\mathrm{e}^-,Ode}\right) - \overleftarrow{k}\theta_{\mathrm{O}^{2-},Ode/g}\left(1-\theta_{\mathrm{O}^{2-},Ode}\right)\theta_{\mathrm{e}^-,Ode}\right\} \tag{17}$$

with rates given as

$$\vec{k} = \overleftarrow{k} = k^0 \exp\left(-\frac{U^{\mathrm{act}}}{\mathrm{k_B}T}\right) \tag{18}$$

The electron flux at the external interfaces is simply $J_{\mathrm{e}^-,Ode\rightarrow\mathrm{O}^{2-}} = -2J_{\mathrm{O}^{2-},Ode\rightarrow Ode/g}$.

For higher dimension order, any other boundaries would have mass insulating boundary conditions. For the Poisson equation, a reference electrostatic potential must be defined. Therefore, one of the external boundaries – here the left-hand electrode – has a grounded electrostatic potential, and the remaining boundaries have free potentials.

The non-configurational component of the electrochemical potential was unavailable and so was assumed constant. Its value may impact interface transfer fluxes but will not affect the qualitative conclusions of this paper. The unconditional mobilities of oxide ions and localized electrons were assumed to be $10^{-10}/k_B T$ and $10^{-8}/k_B T$, respectively, and the correlation factors were assumed to be 1 for simplicity. The activation energy of interface transfer was assumed to be 1 eV, and β was assumed to be 0.5.

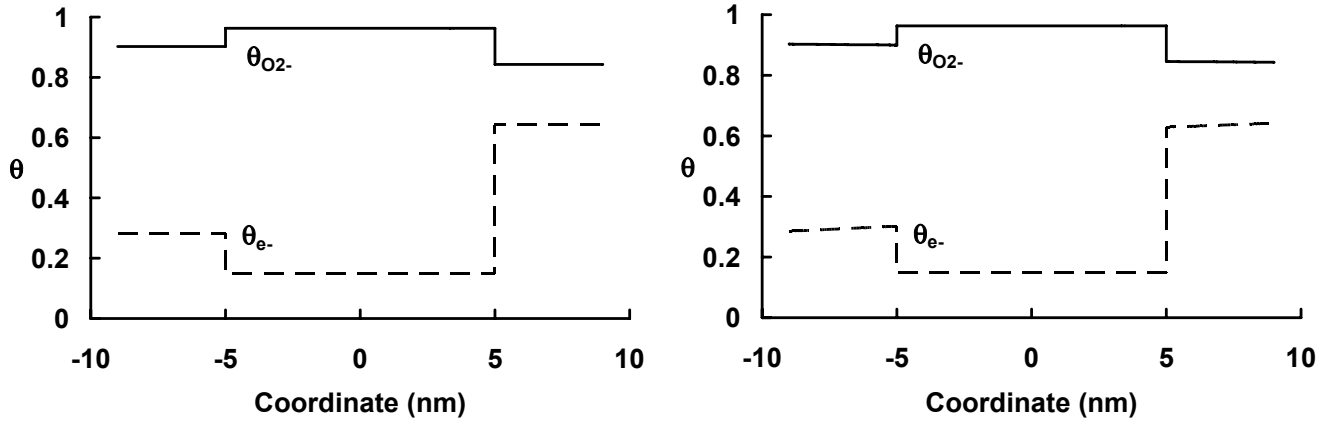

Figure 1: Concentration profiles for a small 1D cell: open-circuit (left) and steady-state (right).

Under open-circuit conditions, a difference in oxygen pressure at the left-hand and right-hand electrodes generates an equilibrium concentration distribution of charged species and a net cell voltage. The left of figures 1, 2, and 3 show the relative concentrations, electrostatic potential, and electrochemical potential profiles, respectively, for a small 1D cell. Of particular interest, the oxide ion electrochemical potential profile at equilibrium is flat, which provides a verification of the numerical approach (see left of figure 3).

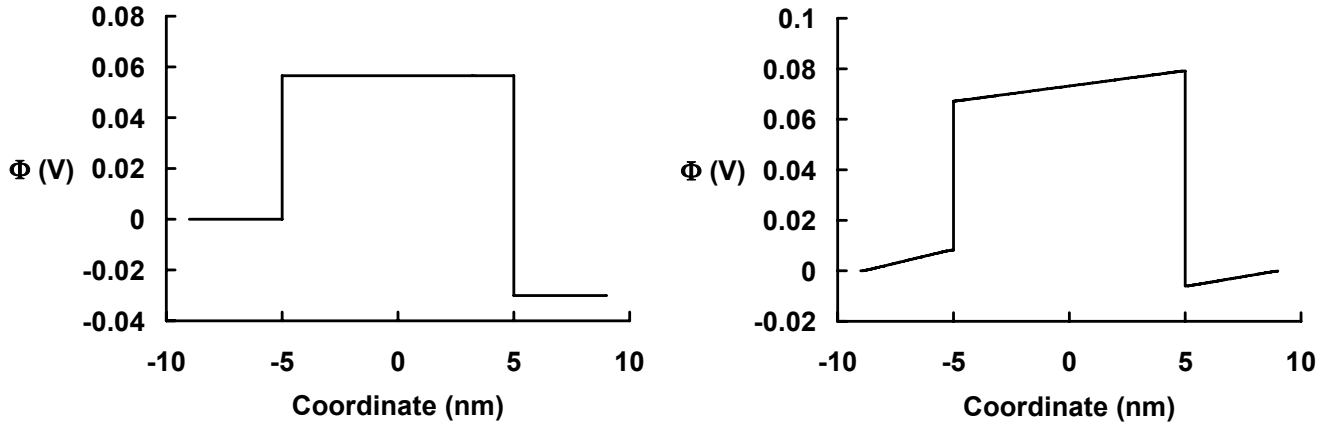

Figure 2: Electrostatic potential profiles for a small 1D cell: open-circuit (left) and steady-state (right).

Under closed-circuit conditions, a steady-state flux is established when a difference in oxygen pressure is applied. The right of figures 1, 2, and 3 show the relative concentrations, electrostatic potential, and electrochemical potential profiles, respectively, for a small 1D cell.

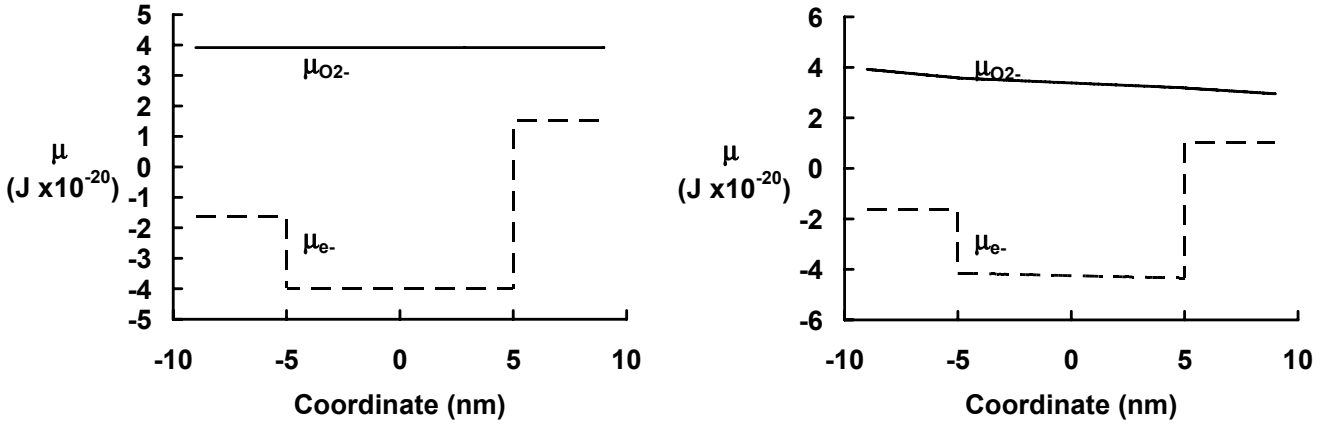

Figure 3: Electrochemical potential profiles for a small 1D cell: open-circuit (left) and steady-state (right).

Comparison of the right-hand figures with the left-hand figures reveals sharp differences between the two conditions. First, the electrochemical potential profile of the oxide ions is no longer flat as indicated in equilibrium, but rather it is markedly sloped downward consistent with a steady-state flux of oxide ions from the left-hand to the right-hand electrode. Second, the concentration profiles are flat in equilibrium, but in steady-state the profiles are no longer entirely flat and exhibit accumulation and depletion regions near the interfaces. These regions are readily seen in figure 4 and take the shape of a diffuse double-layer.

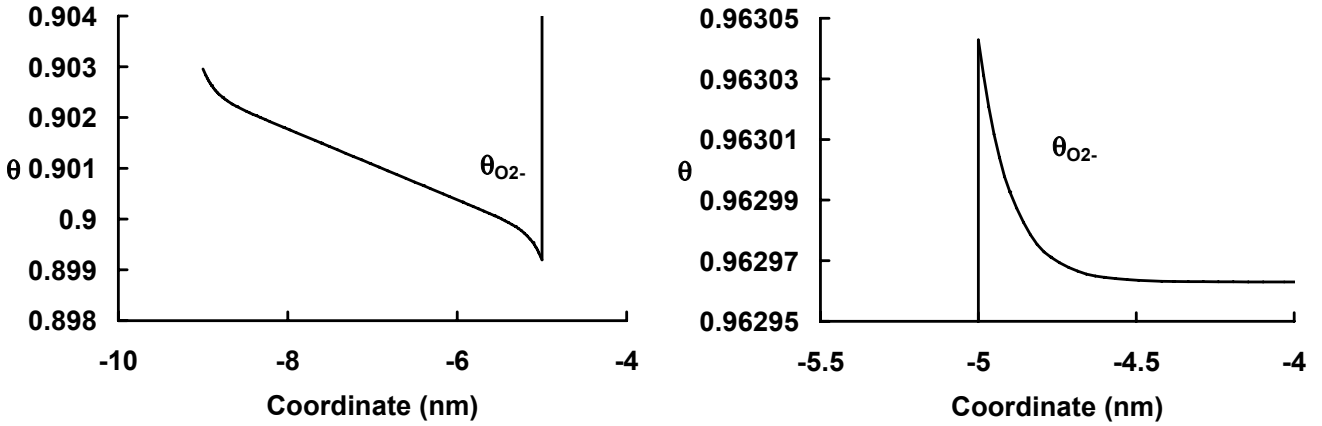

Figure 4: Detail of steady-state relative concentration profiles for a small 1D cell: left-hand side of left-hand electrode/electrolyte interface (left) and right-hand side of left-hand electrode/electrolyte interface (right).

The accumulation region seen in the right-hand part of figure 4 exponentially decays to a constant value. This type of behavior is typically seen in bulk materials and indicates that bulk-like behavior is seen for a 10 nm thick electrolyte membrane. It should be noted that the continuum approximation used here, starts to break down at the 1 nm scale. This does not affect the qualitative conclusions that can be drawn from the results. Transport resistance due to charge accumulation near the interfaces should not be interpreted as interfacial resistance.

Nanoparticles and thin electrolyte synthesis

Zirconia nanoparticles were synthesized by a modified emulsion precipitation method (MEP). Two water-in-oil emulsions were prepared by dispersing 0.02M zirconium chloride or 0.025M hexamethylenetetramine (HMTA) aqueous solutions as droplets in decane by using nonylphenol tetraethyleneglycol ether (Arkopal 40) as surfactant, didodecyldimethylammonium bromide (DiDAB) as co-surfactant, and an Ultra-Turrax dispersion tool (T25, IKA). Both emulsions were mixed and heated for 15 minutes at 60°C while stirring to decompose HMTA into ammonia and formaldehyde. It is believed that the frequent collision of aqueous droplets and exchange through the, temporarily, common surfactant membrane lead to a precipitation reaction between zirconium ions and ammonia, resulting in the formation of zirconium hydroxide inside the aqueous droplets. Poly-octadecyl methacrylate (PODMA) was added as a steric stabilizer, followed by water removal via azeotropic distillation, to achieve steric stabilization of the nanoparticles in the eventual oil phase. The ZrO_2 nanoparticle dispersion via MEP was subsequently purified by removing the precipitation of reaction byproduct NH_4Cl and insoluble surfactant DiDAB from the dispersions. The soluble surfactant Arkopal-40 in the dispersion is further removed by pressure filtration.

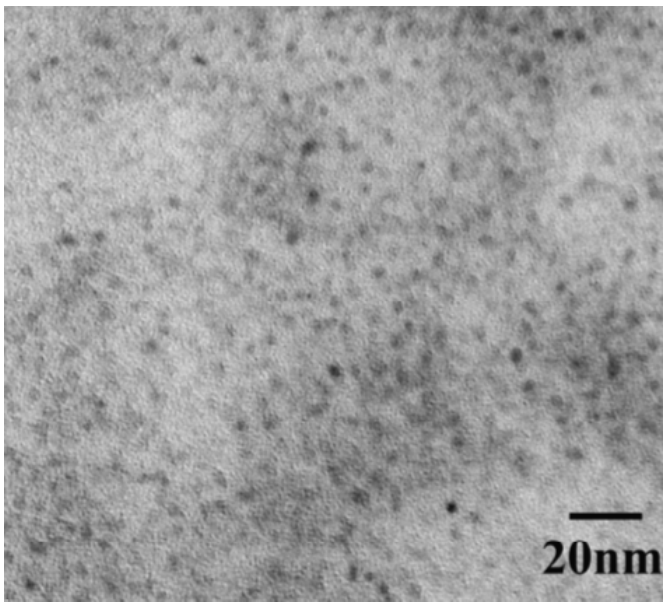

Figure 5: TEM image of non-agglomerated ZrO_2 precursor nanoparticles.

Figure**Error! Reference source not found.** shows a TEM micrograph of ZrO_2 precursor nanoparticles obtained by the MEP method. The particles appear spherical in morphology, non-agglomerated and with a narrow size distribution of 5 nm in diameter. The preparation of a dense zirconia electrolyte can be accomplished by depositing a thin layer of 5 nm zirconia nanoparticles, followed by densification and crystallization. Since the particles are covered with a steric stabilizer layer and well dispersed in decane, they can move independently of each other during the layer formation without the occurrence of agglomeration. This will result in a random-close-packed structure in the as-deposited coating after the evaporation of dispersion medium. The complete densification of random-close-packed, polymer-stabilized spherical 5 nm zirconia particles can take place at near room temperature by oxygen plasma treatment, as shown in figure 6.

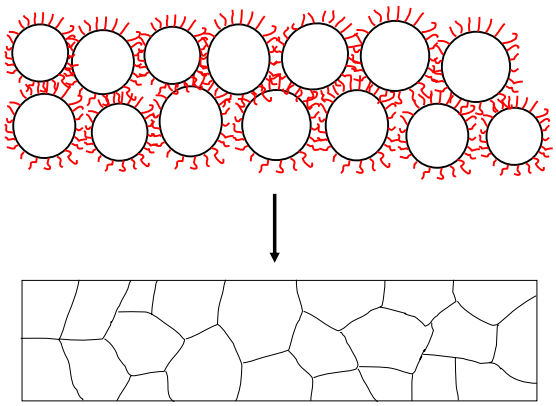

Figure 6: Proposed densification of random-close-packed nanoparticle ensemble, initiated by oxygen plasma treatment.

To enable the preparation of a thin, fully dense ZrO_2 electrolyte layer, a purified dispersion was deposited onto silicon substrates by drops. After drying at room temperature, the coating was heated at 600°C for 3 hours to develop the crystallized structure. Such a ZrO_2 coating was characterized by TEM on a cross-section sample, see figure 7. From electron diffraction, it was confirmed that the coating has crystallized into tetragonal ZrO_2 after heating at 600ºC for 3 hours. The coating appears dense, with an average grain size of 5-10 nm, and adheres very well to the substrate.

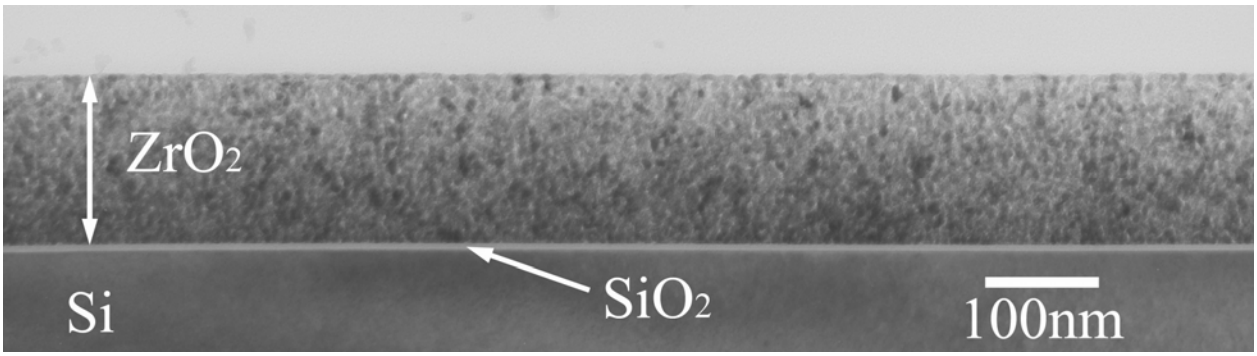

Figure 7: Cross-sectional TEM image of a ZrO_2 coating prepared by direct application and annealed at 600ºC.

Conclusions

Beginning from irreversible thermodynamics and Langmuir site staticstics for mobile species, a model is being developed for the transport processes of solid oxide fuel cells. Though only qualitatively accurate at this time, the model already illustrates the potential for extremely thin electrolyte membrane design. Also, the completed model could allow for better insight into and understanding of experimental measurements, particularly with regard to theoretically unavailable or unattainable constants. The approach as presented might provide a platform for interpretation of complex impedance and I-V measurements in terms of (summed) particle site and activation energies, and (non-configurational) entropies. Possible refinements on the model include:

- Consideration of smaller particle ensembles in interfacial areas where the continuum approach breaks down.
- More realistic chemical potentials.
- Reliable predictions for the correlation coefficients as a function of Φ, θ, and their gradients.

The Langmuir statistics allows all possible co-ordinations of cations by oxygen. The chemical potentials can be made more realistic by using a statistics with plausible restrictions on allowable cation coordinations. Such restrictions would also affect the transport mobility. Coupling of design parameters gleaned from model results with careful and high-definition ceramic processing holds the potential for SOFC with lower fabrication temperatures, greater efficiency and lifetime, and lower operating temperature. The modified emulsion precipitation method as presented has potential as a viable manufacturing route for the foreseen nano-structured electrode/electrolyte configurations.

List of symbols

β: Interfacial transfer symmetry factor.
θ: Time-averaged occupation of a site that is available for one mobile species.
μ: Particle chemical potential, *exclusive* of any $q\Phi$ term.
μ^0: Part of μ, exclusive of partial configurational entropy due to distribution over locations.
$\tilde{\mu}$: Particle chemical potential, *inclusive* of any $q\Phi$ term.
Φ: Electrical potential.
B: Particle mechanical mobility.
B^0: Unconditional *B*. (All neighboring sites are available for diffusion hopping transport).
C_I: Particle concentration.
C_L: Lattice site concentration.
$\tilde{f}_L$: Non-equilibrium correlation coefficient for chemical diffusion on a lattice *L*. In single-component mixtures $0.5 < \tilde{f}_L < 1$ for $\theta \rightarrow 1$ can be expected. In multi-component mixtures $0 < \tilde{f}_{I,L} < 1$; $\tilde{f}_{I,L}$ tends towards unity with decreasing θ.
$\bar{F}$: Thermodynamic driving force.
h: Planck constant.
J: Particle flux.
k^0: Attempt frequency.
k: Rate.
k_B: Boltzmann constant.
K: Equilibrium reaction quotient.
I: Mobile species.
L: Lattice variable.
L_I: Diagonal particle Onsager transport coefficient for species I in systems where all cross-coefficients are 0.
Ode: Electrode variable.
Ode/g: Electrode and gas phase interface.
Ode/Yte: Electrode and electrolyte phase interface.
p: Pressure.
q_{el}: Elementary charge.
T: Temperature.
U^{act}: Activation energy.
v: Particle velocity
Yte: Electrolyte variable.
z: Charge of ionic or electronic species, expressed in terms of q_{el}.